Chapter 8

Stereolithographic fabrication and characterization of immobilized enzyme reactors for *in vitro* digestions

Abstract

Enzymatic digestion is a key process in the gastrointestinal tract, which we recreated in an earlier continuously flowing miniaturized system. In order to avoid the need to continuously supply digestive enzymes, this work studied the immobilization of digestive enzymes in a microsystem. Flow-through reactors were produced by stereolithography and the digestive enzyme, α-amylase, was immobilized onto the channel walls. The activity of immobilized α-amylase was determined by digestion of starch. The resulting immobilized enzyme reactor has potential applications *in vitro* digestions with organ-on-a-chip applications or other enzymatic conversions.

Work in Progress

Pim de Haan[1,2], Maciej Grajewski[1,3], Daan Zillen[1], and Elisabeth Verpoorte[1]

1. University of Groningen, Groningen Research Institute of Pharmacy, Pharmaceutical Analysis, Groningen, the Netherlands.
2. TI-COAST, Amsterdam, the Netherlands.
3. SG Papertronics B.V., Groningen, the Netherlands.

8.1. Introduction

An important step in the development of new drug candidates is the study of the pharmacokinetic behavior of drugs upon oral administration, e.g. when taken as a capsule or tablet. In order to have its action somewhere else in the body, the drug must travel through the mouth, esophagus, and stomach to reach the small intestine, where most absorption of drugs takes place. The drug must therefore be able to withstand the conditions in those organs, including the low pH in the stomach and potential enzymatic conversion. To mimic the processes that occur in the gastrointestinal (GI) tract, *in vitro* digestions simulating the consecutive digestive steps are used to pre-treat samples before transferring them to barrier models of the human intestine, where the eventual absorption may be studied.

In vitro digestions are usually performed in a batch-wise process, in which samples are exposed to artificial digestive juices in test tubes that are rotating for continuous mixing[1,2]. In recent work, we have translated this larger-volume (tens of mL) batch process to a continuous microfluidic digestion-on-a-chip system, with total liquid consumptions reduced to 25 µL/min[3]. Liquid samples were serially exposed to artificial versions of saliva, gastric juice, and intestinal juice and bile in micromixers representing the mouth, stomach, and intestine, respectively. The output of that system, or chyme, was then transferred to a barrier model of the human intestine to study subsequent absorption from the 'gut' compartment into the 'body' compartment of the barrier model[4]. While this system greatly reduced the need for digestive juices, it still required a continuous supply of digestive enzymes as a component of the artificial digestive juices used. This has two drawbacks: the enzymes are the most expensive component of these juices, despite using enzymes of animal or microbial origin; and some enzymes (e.g. proteases) lose activity over time because of autodigestion, which starts reducing their activity from the moment of preparation of the juice throughout the course of an experiment.

Enzymes may therefore be attached to a solid support, using covalent or other bonds[5]. This eliminates the need to continuously supply fresh enzymes in solution. When immobilized onto the surface of beads or the walls of a microfluidic channel, flows of liquid may be created over the enzyme-coated surface, allowing these enzymes to convert substrates contained in the liquid to products[6]. One application of such systems, termed immobilized-enzyme reactors (IMER), is the use of digestive enzymes (usually trypsin) for the pre-treatment of protein samples before mass spectrometric analysis[7]. These systems are highly analogous to digestion

in the human body, and can be modified to better represent the conditions in the GI tract. The activity of immobilized enzymes may be lower due to the immobilization procedure, for example as a result of a block of the active site or steric hindrance from the solid support. Autodigestion, however, will be minimized as the individual enzyme molecules are tethered to the surface and cannot reach adjacent molecules in theory, which conserves the enzyme activity over time[8].

When immobilizing enzymes inside a microfluidic system, special design criteria should be considered based on the kinetics of the enzymes. Reactions of an enzyme (*E*) with a single substrate (*S*) may be represented as follows:

$$E + S \rightleftharpoons E{\cdot}S \rightleftharpoons E + P \qquad (8\text{-}1)$$

In this reaction, an enzyme-substrate complex (*E·S*) is formed before the product (*P*) is formed and released. This first step requires the substrate to come in close proximity with the enzyme, which can be enhanced by using a high concentration of substrate and enzyme. The diffusion distance from the center of the microchannel to the enzyme (immobilized onto the channel wall) should be kept low for minimal diffusion times, thus requiring narrow microchannels. Longer enzyme-substrate exposure times allow for better conversion as well, which requires longer microchannels. The combination of narrow and long channels leads to a high surface-to-volume ratio, providing ample surface area for enzymes to bind[9]. The total surface area may be further increased by placing multiple long, narrow channels in parallel, which leads to a higher enzymatic load inside the device. Finally, the residence time inside the microchannels is determined by the internal volume and the flow rate, so the internal volume must be large enough to accommodate a certain residence time at a set flow rate.

The aim of this study was to develop a microfluidic, immobilized enzyme reactor for use in *in vitro* digestions, taking the specific design considerations above into account. As a first model system, a flow-through microreactor for the oral compartment was selected, recreating the digestion of starch by α-amylase contained in saliva.

8.2. Materials and Methods

All materials were obtained from Sigma Aldrich/Merck (Zwijndrecht, the Netherlands), unless stated otherwise. Water (ultrapure, 18 MΩ·cm) was prepared fresh before each experiment.

8.2.1. Stereolithographic Fabrication

All structures were designed in SolidWorks (Waltham, MA, USA) and printed using an in-house stereolithographic 3D-printer (Form 2, Formlabs, Somerville, MA, USA) using the manufacturer-supplied PreForm 2.16.0 software. Figure 8-1 shows a schematic of the stereolithographic system, with the printing platform above the resin tank. The platform (in the *x*-*y* plane) is lowered into the resin (Clear V4, Formlabs) along the *z*-axis, at a distance of 25 µm above the transparent bottom of the resin tank. A 140-µm laser then illuminates those areas that should be polymerized, leaving a solid material on the printing platform. Additional layers are added onto the previous layer, with the oldest layer attached to the platform and the newest layer at the bottom end of the suspended object. To improve adhesion to the platform, structures were printed with onto a 2-mm-thick base on the printing platform. The actual structure was spaced at 5 mm from this base, suspended by an array of support pillars (which were removed at the end of the fabrication process). The locations of these pillars were generated by the software to provide ample support, and if needed, the location of pillars to be printed was changed manually to prevent pillars blocking essential structures of the print (e.g. channel entrances, or thread).

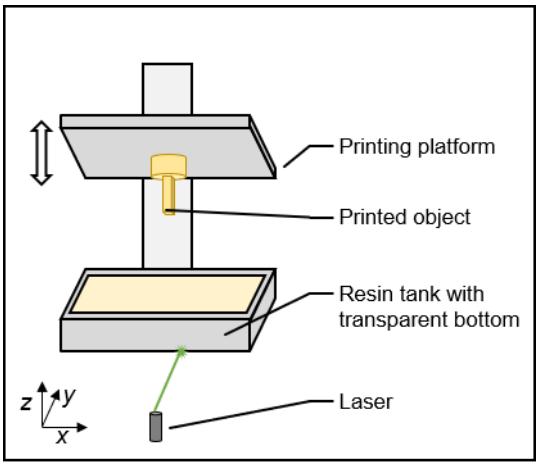

Figure 8-1 Schematic of the stereolithographic fabrication. A printing platform moves down (in the z-direction) into the resin tank in order for the laser to cure another layer of material onto the printed object. The print thus grows on the platform, with the newest layers at the bottom. The axes are labeled at the bottom left for clarity.

All prints were processed according to the manufacturer's guidelines. Excess resin was removed from microchannels using compressed air. The remaining resin was removed by immersion in isopropanol for 15 min, followed by another 5 min immersion in fresh isopropanol. For structures containing connectors with thread, such as isometric M5 thread, male and female parts were screwed together before drying to ensure optimal fit. After drying on a tissue in the fume hood and blowing microchannels dry with compressed air, the prints

were UV-cured at 60°C for 30 min (FormCure, Formlabs). Print bases and supports were then removed from the final structure, removing fine pillar remnants with sandpaper. The final prints were visually inspected using stereomicroscopes.

8.2.2. Solvent Compatibility

The solvent compatibility of the prints was studied by full immersion in water, dimethyl sulfoxide (DMSO), methanol, ethanol, and hexane, in closed glass containers. Dilutions of ethanol and DMSO (10% in water) were tested as well. Cubes of approximately 10 mm containing microchannels were incubated in these solvents for 1 and 24 h, and the objects were inspected visually for potential damage.

8.2.3. Enzyme immobilization

Enzymes were immobilized onto the walls of the printed column with microchannels according to a modified literature procedure[10]. The prints consisted of a poly(methyl methacrylate) (PMMA)-like material, which was oxidized using oxygen plasma (2 min at 29 W; Harrick Plasma PDC-0002, Ithaca, NY, USA) (Figure 8-2, step a). The following steps were performed by loading liquids with the necessary reagents in syringes, and using a syringe pump (ProSense NE-1000, Oosterhout, the Netherlands) to establish flows. The hydroxyl moieties generated by the plasma oxidation could be used to covalently attach 3-aminopropyltriethoxysilane (APTES, 2% in hexane, 5 µL/min for 30 min), yielding a free primary amine on the surface (step b). The column was washed with pure hexane to remove excess reagents and dried with compressed air. Glutaraldehyde (5% in phosphate-buffered saline, pH 7.2, 5 µL/min for 10 min) was introduced under formation of a Schiff base with the primary amine group (step c). After removing excess reagent with fresh phosphate-buffered saline, α-amylase (from *Bacillus* sp., 1 mg/mL in water) was introduced at 600 µL/min for 2 min. The flow was then adjusted to 5 µL/min for 30 min to allow the enzyme to attach covalently to the reactive aldehyde groups (step d). The column was then extensively rinsed with artificial saliva without enzymes (as described in earlier work[3]) and connected to fresh tubing (poly(tetrafluoroethylene), 1.6/0.8 mm inner/outer diameter, Polyfluor Plastics, Breda, the Netherlands), needles (21G, BD, Vianen, the Netherlands), and syringes (Omnifix 5 mL, Braun Medical, Oss, the Netherlands) for further studies. As a non-active control, the same procedure was used to immobilize bovine serum albumin (BSA, 1 mg/mL in water) in columns.

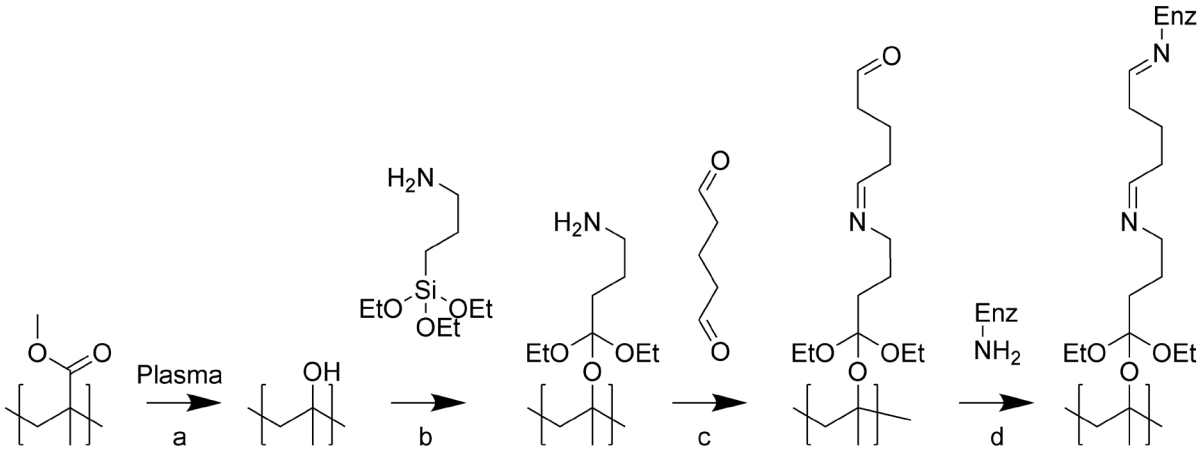

Figure 8-2 Immobilization procedure for proteins such as enzymes. The 3D-printed material consists of methacrylate monomers, which contain methyl ester groups on the surface. a) An oxygen plasma treatment oxidizes the surface, yielding free hydroxyl groups. b) The silane, APTES, is introduced to form ether bonds to the surface. c) Glutaraldehyde covalently bonds to the amine moiety of the APTES molecule. d) The second aldehyde group is available for binding to any primary amine of any protein or enzyme, yielding a covalent link between the immobilized protein and the surface.

8.2.4. Enzyme Kinetics

The activity of immobilized α-amylase and BSA was determined by exposing the column to varying concentrations of quenched, fluorescently labeled starch (EnzChek Ultra Amylase, ThermoFisher, Breda, the Netherlands), prepared fresh according to the manufacturer's instructions. A dilution series of this starch in artificial saliva (without enzyme) was prepared (at 1, 2.5, 5, 10, 15, 25, 40 µg/mL), and stored protected from light until further use. The assay started by assembling a fresh immobilized enzyme reactor (~292 µL internal volume) with all necessary syringes and tubing, and introducing the lowest concentration of starch using a syringe. The residence time was then increased gradually (starting with 5 s, then 10 s, 20 s, 40 s, 60 s, and 90 s), with effluents collected after each step. The first series of samples were collected using 1 µg/mL starch, and then a higher concentration of starch was introduced by flow. Starch that had not been passed through the column was used as a "0 s" control sample. The fluorescence of the samples was measured using a fluorimeter (excitation/emission 485/538 nm; Gemini XPS, Molecular Devices, San Jose, CA, USA), with higher fluorescence levels indicating the presence of higher levels of reaction products. This entire process was performed in triplicate for α-amylase and BSA, and the increase in fluorescence from the "0 s" control to the 5-s sample was used as a measure for the initial reaction rate.

8.3. Results and Discussion

8.3.1. Printing Orientation and Resolution

As the stereolithographic system used creates structures layer by layer, the resolution of prints is determined by two different factors: in the *x*- and *y*-dimensions, the 140-µm spot size of the laser that cures the resin determines the minimum feature size[11]. The *z*-dimension is determined by the movements of the printing platform, with a minimum layer thickness of 25 µm (Figure 8-1). Therefore, the resolution in the *z*-direction seems to be better than those in the *x*- and *y*-directions, but it was found that cavities could be printed better in the *z*-direction (perpendicular to the printing platform). When printing cavities (i.e. open channels) along the *z*-axis, their outlines were sharp and the channels remained open, whereas if channels were printed on the *x,y*-plane, outlines contained zig-zag walls caused by the layer-by-layer printing, and even though the layer thickness was 25 µm, cavities of only one or a few layers were obstructed, presumably partially cured by the laser curing the subsequent layers. Therefore, all porous structures were printed with their cavities along the *z*-axis of the stereolithographic printer.

Cylindrical pores of 10-mm length and different diameters were printed to determine the smallest possible channel size for microfluidic structures (Figure 8-3, left panel). Pores with a diameter of at least 700 µm were open after fabrication and development of the printed structures, and those with a diameter of 650 µm and lower were obstructed by partially cured resin. Therefore, channels of 700-µm diameter were selected for use in the microfluidic system. The inter-channel wall thickness was varied from 140 µm to 200 µm in steps of 10 µm to find the optimum wall thickness. Only in the case of 200-µm thick walls (heart-to-heart spacing 900 µm), it was found that all channels were open after fabrication (Figure 8-3, right panel). Apparently, even though the laser spot size is 140 µm, some resin directly adjacent to the illuminated area is affected by the laser and cured partially. A column with 70 10-mm-long channels was selected for further studies, with 700-µm diameter channels and 200-µm spacing, leading to a porosity of 55% calculated from the cross-sectional area.

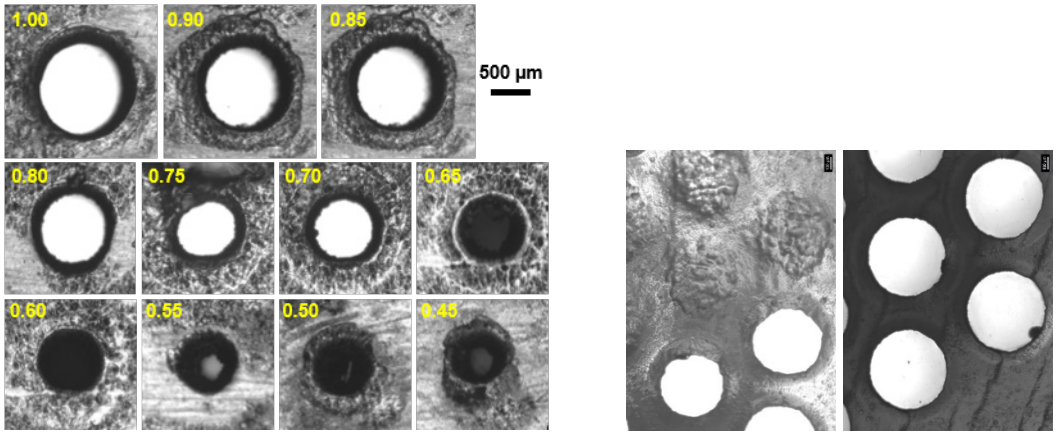

Figure 8-3 Left: Cylindrical pores were printed along the z-axis of the printer. The pore diameter is displayed in mm, with open channels indicated by a light-colored internal volume. Channels of 0.65 mm and under were blocked by partially cured resin (appearing black). Note that the channel outlines also became more rugged at lower diameters. Right: The effect of inter-channel wall thickness of 700-µm-wide channels (10 mm long), printed with 140 µm (left micrograph) or 200 µm wall thickness (right micrograph). Some channels were obstructed when using 140-µm walls, whereas all channels were open with a 200-µm wall thickness (same scale).

8.3.2. Solvent Compatibility

The exact composition of the printed material is not known, but the final prints consist of a poly(methyl methacrylate) (PMMA)-like material[12]. The printed materials were found to have a solvent resistance that is very similar to PMMA (Table 8-1). The material was compatible with water and hexane, but the printed structures showed signs of damage after submersion in pure ethanol, methanol, and dimethyl sulfoxide (DMSO). The structures were swollen and

Table 8-1 Compatibility of 3D-printed objects with several different solvents, after 1-h and 24-h exposure to the solvent. +: Compatible, no visual effects of degradation. +/-: Some non-destructive effects visible. Increased translucence was observed after quickly drying the objects, and comparing to a non-treated control object. -: Incompatible; severe damage to 3D-printed objects visible.

Solvent	Exposure time		Observations
	1 h	24 h	
Dimethyl sulfoxide, pure	+/-	-	Increased translucence without structural damage after 1 h. Severe damage, swelling and formation of cracks after 24 h.
Dimethylsulfoxide, 10% in water	+	+/-	No visible effects after 1 h. Increased translucence without structural damage after 24 h.
Ethanol, 96%	-	-	Severe structural damage, swelling, and formation of cracks within 1 h.
Ethanol, 10% in water	+	+	No visible effects.
Hexane	+	+	No visible effects.
Methanol, pure	-	-	Severe structural damage, swelling, and formation of cracks within 1 h.
Water, pure	+	+	No visible effects.

showed signs of cracks even after only 1 h of incubation in these solvents. Diluted ethanol and DMSO (10% in water) showed no effects after 1 h, and only minor damage became apparent after 24 h of incubation in 10% DMSO.

8.3.3. Fabrication of Modular Microfluidic Elements

Several different microfluidic elements were fabricated by stereolithography (Figure 8-4). The static mixer (panel A) consisted of two inlets and one common outlet, and contained semi-elliptical structures printed inside a cylindrical channel (diameter 1.5 mm, length 12 mm) to perturb flows. The semi-elliptical flow perturbation elements were placed at a 45-degree angle with respect to the channel, and at 90-degree angles between two adjacent elements. The mixing behavior could not be quantified, but full mixing of blue and yellow dyes was apparent with visual inspection over a range of flow rates (1 – 100 µL/min total flow rate). The static mixer contained three male Luer connectors, that could be connected to other elements or 21G needles with Luer female connectors[13]. Wider elements were connected with metric M5 standardized thread[14]. Panel B shows a flow-through column with two connectors: the top

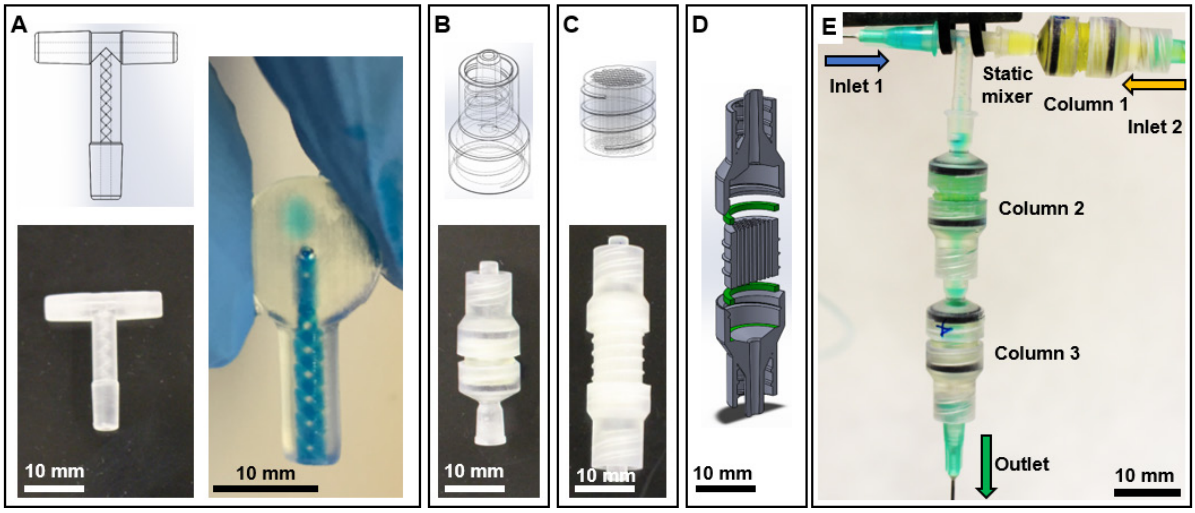

Figure 8-4 Several different fluidic elements were fabricated. A) Static mixer, containing an array of semi-elliptical elements placed at a 45-degree angle to the longitudinal axis and alternating at a 90-degree angle from one element to the next. B) Several fluidic connectors, including Luer-compatible male (top in both the 3D-rendering and the photograph) and female (bottom in the photograph) connectors and M5-standardized thread to connect larger objects (bottom half of the 3D-rendering). C) Porous columns with micrometer-sized channels inside and an outside M5-standardized thread. D) Exploded and cross-sectional view of a porous column, with two O-rings (green), and two Luer male-to-M5 connectors to connect the set-up. E) Photograph of an assembly of different elements: two pumps (not shown) supply solutions of blue (top left, inlet 1) and yellow (top right, inlet 2) food dye. Solution 2 is passed through a first column before being mixed with solution 1 by a static mixer, yielding a green-colored solution. The solution then passes through columns 2 and 3 toward the outlet (bottom). The 3D-printed fluidic objects are somewhat transparent, visible by colors of the solutions showing through. O-rings were printed using a different (flexible) resin, and these are visible as black rings. Needles (shown in light green) were used to connect PTFE tubing to the Luer connectors.

element is a Luer male-to-M5 connector, the bottom element an M5-to-Luer female connector. All flow elements could be connected to one another without leakage, with printed flexible O-rings between the M5 connectors for extra leakage-proofing (green in Panel D). An assembly of several different elements is shown in Panel E; a whole range of other passive and active fluidic elements may be printed and included as well.

8.3.4. Enzyme Immobilization

The effectiveness of the immobilization procedure was confirmed by changes in the water contact angle. The effectiveness of the immobilization procedure was confirmed by measuring changes in water contact angles (n = 3) from 68.4±1.9° (printed material) to 43.5±2.3° (after plasma treatment) to 48.2±3.1° (after APTES coating). The lower contact angle after oxygen plasma treatment was expected, as hydroxyl moieties are introduced on the surface by the oxidative action of the plasma[15]. Coating with APTES yielded a similarly hydrophilic surface, as the introduction of amine groups on the surface render it somewhat hydrophilic[10]. The water contact angle was not determined after glutaraldehyde treatment, as this compound is unstable when only bound to the surface on one end, and the other end may form bonds to other groups on the surface upon washing and drying.

8.3.5. Enzyme Kinetics

As a first demonstration of an immobilized enzyme reactor for use in *in vitro* digestions, a flow-through reactor consisting of a 10-mm-long porous column was surface-treated and the enzyme, α-amylase, was immobilized onto the channel walls. Quenched fluorescently labeled starch was supplied as a substrate, and the initial reaction rate was measured at various different concentrations of starch (substrate). As a non-active control, bovine serum albumin (BSA) was immobilized in a different column and subjected to the same enzymatic starch assay to exclude background effects by the column materials, connectors, or possible contaminations (Figure 8-5). The measured profiles showed a Michaelis-Menten-like kinetic behavior in the case of α-amylase, and no catalytic effects were found using BSA. The conversion of starch to fluorescent oligosaccharides must therefore be catalyzed by the immobilized α-amylase, indicating that the enzymes were indeed immobilized as they did not elute from the column upon extensive washing steps. The activity was retained upon immobilization, although the exact activity (e.g. in units per column) could not be quantified as arbitrary fluorescence units are measured. A saturation of the immobilized enzymes could not be detected, even at the

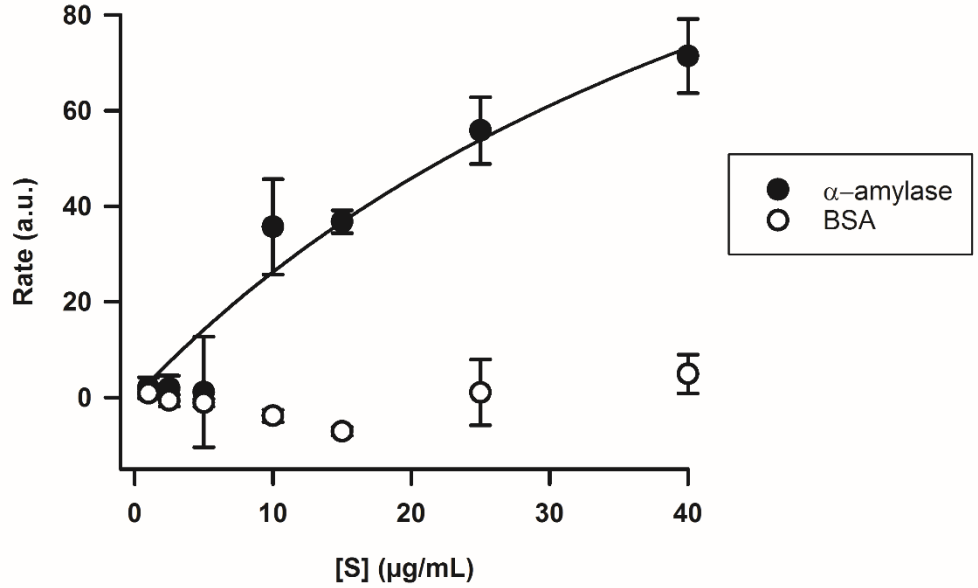

Figure 8-5 Kinetic plot of the breakdown of fluorescently labeled starch by immobilized α-amylase (black circles) or immobilized bovine serum albumin (BSA, control, white circles). The fitted curve can only be used as some indication of the kinetics, as saturation was not reached at the highest concentration of starch. The mean of the initial reaction rate (initial 5 s) in three separate experiments (n = 3) is plotted, with error bars representing the standard deviation.

highest concentration of starch that was supplied to the column. It is possible that the activity of immobilized enzymes is lower than usual due to possible blocking of the active site or other crucial elements of some of the individual enzyme molecules. A more thorough evaluation of the amount of enzyme immobilized (weight or moles) and a calibration of the kinetic assay to exact units would be necessary in order to obtain that information. The stability of the immobilized enzymes is still unknown; this too should be determined to allow for longer-term or multiple use in the future. The comparison with immobilized BSA, in this case, demonstrates that the observed enzymatic activity is no 'aspecific' catalysis that could be done by another protein, nor that it is occurring as a result of catalysis or other action by the printed material or the chemicals used in the immobilization procedure and other contaminants.

8.4. Conclusion

Stereolithography was used to produce modular microfluidic elements, which could be connected to one another in a leak-free manner using Luer and M5 connections. A 10-mm-long column with 70 straight cylindrical microchannels of 700 µm diameter and 200-µm-thin inter-channel walls could be produced reliably and robustly. The enzyme, α-amylase, was immobilized onto the channel walls, and the activity of this enzyme was confirmed by experiments with various concentrations of quenched, fluorescently labeled starch. The exact

enzymatic activity nor the longer-term stability of the enzymes has been determined yet, but since activity is present, the immobilization strategy may be optimized to achieve the exact needed amount of enzymatic activity to function as 'oral digestion compartment' in a flow-through *in vitro* digestive system, greatly reducing the need for digestive enzymes in *in vitro* digestions. It is expected that this immobilization strategy could also be used for enzymes of other digestive compartments (e.g. stomach and intestine), as well as other analytical, catalytic and possibly biocatalytic purposes.

8.5. Acknowledgments

We thank Kelci M. Schilly (University of Kansas) for her contributions and insightful discussions. This project received funding from the Dutch Research Council (NWO, PTA-COAST3, Project number 053.21.116, 'GUTTEST').

8.6. References

1 M. Minekus, M. Alminger, P. Alvito, S. Ballance, T. Bohn, C. Bourlieu, F. Carrière, R. Boutrou, F. M. Corredig, D. Dupont, F. C. Dufour, L. Egger, M. Golding, L. S. Karakaya, B. Kirkhus, S. Le Feunteun, U. Lesmes, A. Macierzanka, A. Mackie, S. Marze, D. J. McClements, O. Ménard, I. Recio, C. N. Santos, R. P. Singh, G. E. Vegarud, M. S. J. Wickham, W. Weitschies and A. Brodkorb, *Food Funct.*, 2014, **5**, 1113–1124.

2 A. Brodkorb, L. Egger, M. Alminger, P. Alvito, R. Assunção, S. Ballance, T. Bohn, C. Bourlieu-Lacanal, R. Boutrou, F. Carrière, A. Clemente, M. Corredig, D. Dupont, C. Dufour, C. Edwards, M. Golding, S. Karakaya, B. Kirkhus, S. Le Feunteun, U. Lesmes, A. Macierzanka, A. R. Mackie, C. Martins, S. Marze, D. J. McClements, O. Ménard, M. Minekus, R. Portmann, C. N. Santos, I. Souchon, R. P. Singh, G. E. Vegarud, M. S. J. Wickham, W. Weitschies and I. Recio, *Nat. Protoc.*, 2019, **14**, 991–1014.

3 P. de Haan, M. A. Ianovska, K. Mathwig, G. A. A. van Lieshout, V. Triantis, H. Bouwmeester and E. Verpoorte, *Lab Chip*, 2019, **19**, 1599–1609.

4 P. de Haan, M. J. C. Santbergen, M. van der Zande, H. Bouwmeester, M. W. F. Nielen and E. Verpoorte, *Sci. Rep.*, 2021, **11**, 4920 (2021).

5 Y. Asanomi, H. Yamaguchi, M. Miyazaki and H. Maeda, *Molecules*, 2011, **16**, 6041–6059.

6 M. Safdar, J. Spross and J. Jänis, *J. Chromatogr. A*, 2014, **1324**, 1–10.

7 B. Wouters, B. W. J. Pirok, D. Soulis, R. C. Garmendia Perticarini, S. Fokker, R. S. van den Hurk, M. Skolimowski, R. A. H. Peters and P. J. Schoenmakers, *Anal. Chim. Acta*, 2019, **1053**, 62–69.

8 C. Wang, A. B. Jemere and D. J. Harrison, *Electrophoresis*, 2010, **31**, 3703–3710.

9 H. Bruus, *Theoretical Microfluidics*, Oxford University Press, Oxford, UK, 2008.

10 Ł. Syga, D. Spakman, C. M. Punter and B. Poolman, *Sci. Rep.*, 2018, **8**, 1–12.

11 Formlabs Inc., Form 2 Tech Specs, https://formlabs.com/eu/3d-printers/form-2/tech-specs/, (accessed June 12, 2021).

12 Formlabs, 2021. Clear resin safety data sheet (accessed June 12, 2021).

13 International Organization for Standardization, *ISO 594-2:1998*, 1998.

14 International Organization for Standardization, *ISO 68-1:1998*, 1998.

15 L. Brown, T. Koerner, J. H. Horton and R. D. Oleschuk, *Lab Chip*, 2006, **6**, 66–73.